Effects of hydration on the elastic properties of olivine

Steven D. Jacobsen,[1] Fuming Jiang,[2] Zhu Mao,[2] Thomas S. Duffy,[2] Joseph R. Smyth,[3] Christopher M. Holl,[1] and Daniel J. Frost[4]

Received 25 April 2008; revised 12 June 2008; accepted 17 June 2008; published 18 July 2008.

[1] Water, dissolved as hydroxyl $(OH)^-$ into the solid silicate minerals of the upper mantle can reduce adiabatic wave speeds through associated defects. Here we report Brillouin spectroscopy measurements of the sound velocities and single-crystal elastic constants of hydrous forsterite (hy-Fo_{100}) and hydrous olivine (hy-Fo_{97}) containing 0.8–0.9 wt% H_2O. The samples, synthesized at 12 GPa and 1250°C, represent nearly the maximum storage capacity of water in olivine at conditions of 350–400 km depth. The adiabatic bulk (K_{S0}) and shear (G_0) moduli of hy-Fo_{100} are 125.7(±0.2) GPa and 79.8(±0.1) GPa, respectively. For hy-Fo_{97}, we obtain K_{S0} = 124.4(±0.4) GPa and G_0 = 75.3(±0.3) GPa. Compared with anhydrous forsterite, the combined effects of 3 mol% Fe and 0.8 wt% H_2O reduce bulk and shear moduli by 3.5(±0.3)% and 7.5(±0.4)% respectively, with greater reductions expected for more iron-rich Fo_{90} mantle compositions. Although lattice preferred orientation (LPO) studies have not been carried out under relevant conditions of water or pressure, analysis of idealized single-crystal anisotropy for various known LPO types predicts up to 3% higher S-wave splitting anisotropy in hydrous olivine crystals aligned according to A-type and E-type fabrics, but no change in S-wave splitting anisotropy for B-type and C-type fabrics. **Citation:** Jacobsen, S. D., F. Jiang, Z. Mao, T. S. Duffy, J. R. Smyth, C. M. Holl, and D. J. Frost (2008), Effects of hydration on the elastic properties of olivine, *Geophys. Res. Lett.*, *35*, L14303, doi:10.1029/2008GL034398.

1. Introduction

[2] Hydrogen-related defects are known to influence the physical properties of mantle materials. Of particular relevance to geophysical studies are the effects of hydration on rheology [e.g., *Mei and Kohlstedt*, 2000; *Jung et al.*, 2006], elasticity [e.g., *Jacobsen*, 2006], anelasticity [e.g., *Karato and Jung*, 1998], melting [e.g., *Hirth and Kohlstedt*, 1996] and electrical conductivity [e.g., *Simpson and Tommasi*, 2005]. Because the water-storage capacity of olivine approaches 1 wt% H_2O at depths of 350–400 km [e.g., *Smyth et al.*, 2006], the effects of hydration on the elastic properties of olivine are needed to evaluate seismic anomalies in the upper mantle that are not easily explained by temperature alone [e.g., *Karato*, 1993].

[3] Studies of hydrogen partitioning between upper mantle minerals and silicate melts at high-pressures and temperatures indicate that the water storage capacity of model peridotite is about 0.6 wt% at 410 km [*Hauri et al.*, 2006]. *Mosenfelder et al.* [2006a] synthesized iron-bearing olivine at 12 GPa and 1100°C containing 0.64 wt% H_2O, and *Litasov et al.* [2007] reported 0.63 wt% H_2O in olivine at 12.5 GPa and 1200°C. At 12 GPa, the water storage capacity of olivine decreases from a maximum of about 0.9 wt% H_2O above 1300°C [*Smyth et al.*, 2006]. In addition to temperature, water storage capacity depends on oxygen and water fugacity [e.g., *Mosenfelder et al.*, 2006a], silica activity [e.g., *Lemaire et al.*, 2004] and the incorporation of Al [*Hauri et al.*, 2006] and Fe [*Zhao et al.*, 2004].

[4] The defect structure and hydration mechanisms of olivine have been studied mainly by single-crystal X-ray diffraction, and inferred from polarized FTIR spectroscopy, and these have been reviewed along with new observations from electron microscopy by *Mosenfelder et al.* [2006b]. X-ray structure refinements of hydrous olivine show mainly evidence for Mg^{2+} site vacancies [e.g., *Smyth et al.*, 2006], whereas FTIR studies of hydrous olivine grown under varying silica activity suggest hydration mechanisms involving both Mg^{2+} and Si^{4+} vacancies [e.g., *Lemaire et al.*, 2004; *Mosenfelder et al.*, 2006a; *Litasov et al.*, 2007].

[5] This paper deals mainly with the effects of hydration on elastic properties, without analysis of the olivine defect structure. Water is known to significantly reduce the elastic moduli of high-pressure olivine polymorphs, wadsleyite (β-Mg_2SiO_4), and ringwoodite (γ-Mg_2SiO_4). The elastic moduli of Mg-end member hydrous wadsleyite containing 1 wt% H_2O show a 7.6% reduction in the bulk (K_{S0}) and 7.0% reduction in shear (G_0) moduli [*Mao et al.*, 2008]. The elastic moduli of Mg-end member hydrous ringwoodite containing 2.3 wt% H_2O was studied to 23.4 GPa by Brillouin spectroscopy and show a reduction of 9% in the bulk and shear moduli compared with anhydrous Mg-ringwoodite [*Wang et al.*, 2006]. The elastic properties of hydrous Fo_{90}-ringwoodite containing 1 wt% H_2O were measured by GHz-ultrasonic interferometry to 10 GPa, showing a 4.3% reduction of K_{S0} and 14% reduction in G_0 compared with anhydrous Mg-ringwoodite [*Jacobsen and Smyth*, 2006]. Because the addition of iron to anhydrous Mg_2SiO_4 polymorphs has a small, or slightly positive (increasing) effect on K_S, but strongly reduces G [e.g., *Sinogeikin et al.*, 1998], the net effect of adding iron and water to Mg-silicates is predominantly on shear properties, and consequently Vp/Vs ratios.

[6] The high water storage capacity of olivine at mantle conditions near the transition zone warrants investigation of

[1]Department of Earth and Planetary Sciences, Northwestern University, Evanston, Illinois, USA.
[2]Department of Geosciences, Princeton University, Princeton, New Jersey, USA.
[3]Department of Geological Sciences, University of Colorado, Boulder, Colorado, USA.
[4]Bayerisches Geoinstitut, University of Bayreuth, Bayreuth, Germany.

0094-8276/08/2008GL034398

Table 1. Elastic Properties of Olivine with Varying Iron and Water Content[a]

	Forsterite[b]	San Carlos Olivine[c]	Effect of Fe (%)[d]	Hy-Fo100[e]	Effect of H_2O (%)[d]	Hy-Fo97[e]	Effect of Fe and H_2O (%)[d]
Mg#	1.00	0.90		1.00		0.97	
H_2O (wt%)[f]	0	0		0.89		0.80	
C_{ij} (GPa)							
C_{11}	328.6(5)	320.2(4)	−2.6	315.4(6)	−4.0	306.7(14)	−6.7
C_{22}	200.1(3)	195.9(3)	−2.1	195.3(5)	−2.4	191.9(11)	−4.1
C_{33}	235.7(5)	233.8(3)	−0.8	234.4(7)	−0.6	227.2(20)	−3.6
C_{12}	66.8(3)	67.9(3)	+1.6	64.8(6)	−3.0	63.8(15)	−4.5
C_{13}	68.4(4)	70.5(3)	+3.1	67.2(6)	−1.8	67.9(13)	−0.7
C_{23}	72.7(3)	78.5(4)	+8.0	70.2(6)	−3.4	73.3(14)	+0.8
C_{44}	67.0(1)	63.5(2)	−5.2	66.0(3)	−1.5	62.0(8)	−7.5
C_{55}	81.2(2)	76.9(2)	−5.3	80.2(2)	−1.2	76.3(6)	−6.0
C_{66}	80.9(1)	78.1(1)	−3.5	78.7(4)	−2.7	71.6(9)	−11.5
ρ (kg/m^3)	3225	3350	+3.9	3180(3)	−1.4	3240(3)	+0.5
K_{S0} (GPa)	128.9	129.5	+0.5	125.7(2)	−2.5	124.4(4)	−3.5
G_0 (GPa)	81.4	77.5	−4.8	79.8(1)	−2.0	75.3(3)	−7.5
V_P (km/s)	8.58	8.34	−2.8	8.54(1)	−0.5	8.33(1)	−2.9
V_S (km/s)	5.02	4.81	−4.2	5.01(1)	−0.2	4.82(1)	−4.0
V_P/V_S	1.709	1.733	+1.4	1.705(5)	−0.3	1.728(6)	+1.1
Poisson, ν	0.239	0.251	+5.0	0.238(7)	−0.4	0.248(7)	+3.6

[a]Values in parentheses are standard deviations in the last place.
[b]*Suzuki et al.* [1983].
[c]*Webb* [1989].
[d]Percent change compared with anhydrous forsterite.
[e]This study.
[f]Water contents estimated using the calibration of *Bell et al.* [2003].

the effects of hydration on its elastic properties. Here we report the elastic properties hydrous forsterite (hy-Fo_{100}) and hydrous olivine (hy-Fo_{97}) containing what is considered to be the maximum possible concentration of water (0.9 wt% H_2O) in olivine. The results, along with previous elasticity data for minerals along the olivine-brucite join, provide constraints on the effects of hydration on the elastic moduli and sound velocities.

2. Experimental and Analytical Methods

[7] Hydrous olivine crystals were synthesized in the 5000-tonne multianvil press at Bayerisches Geoinstitut [*Smyth et al.*, 2006]. The forsterite composition (hy-Fo_{100}) corresponds to run SZ0408A, and the iron-bearing composition (hy-Fo_{97}) corresponds to run SZ0407B of *Smyth et al.* [2006]. Both runs were carried out at 12 GPa and 1250°C (~360 km depth), but the hy-Fo_{100} samples equilibrated with enstatite and melt, whereas the Fe-bearing hy-Fo_{97} composition equilibrated with clinohumite and melt. Thus, the hy-Fo_{100} and hy-Fo_{97} samples were annealed under conditions of relatively high, and low silica activity, respectively. Polarized FTIR measurements employing the calibration of *Bell et al.* [2003] were used to determine the water contents of the hy-Fo_{100} (0.89 wt% H_2O) and hy-Fo_{97} (0.80 wt% H_2O) samples (Table 1).

[8] For the Brillouin scattering measurements, 100–250 μm sized grains with optical clarity and clean extinction in cross-polarized light were oriented on a four-circle X-ray diffractometer. Plates parallel to (100), (010), and (001), and several randomly oriented grains were prepared for each composition. Crystals were double-polished (parallel faces) to 40–70 μm thickness, and 100–250 μm lateral dimensions. Brillouin spectra were obtained using a single-frequency, vertically polarized neodymium vanadate laser (λ = 532.15 nm) with a power of 150 mW at the sample using a six-pass Sandercock tandem Fabry-Perot interferometer in a forward symmetric scattering geometry. Acoustic velocities were determined by:

$$V = \frac{\Delta\nu_B \lambda_0}{2\sin(\theta/2)}, \quad (1)$$

where, λ_0 is the incident laser wavelength, $\Delta\nu_B$ is the measured Brillouin frequency shift and θ is the scattering angle external to the cell, which was 70(±0.03)° in this study. Each platelet was rotated about the axis bisecting the incident and collected light path and spectra were obtained every 5–10°, resulting in up to 28 velocity measurements (Vp and Vs) in each plane (Figure 1).

3. Results and Discussion

[9] The Christoffel equations [e.g., *Every*, 1980] were fitted to the measured phonon velocities and Eulerian angles defining the crystal orientation. Olivine is orthorhombic with nine non-zero elastic constants: C_{11}, C_{22}, C_{33}, C_{12}, C_{13}, C_{23}, C_{44}, C_{55} and C_{66}. For the hy-Fo_{100} composition, three platelets were measured with three Eulerian angles each, plus the nine elastic constants, totaling 18 parameters to fit. We used X-ray densities of 3180(±3) kg/m^3 for the hy-Fo_{100} and 3240(±3) kg/m^3 for the hy-Fo_{97} [*Smyth et al.*, 2006]. We note that hydration of forsterite to 0.89 wt% H_2O reduces its density by about 1.4% compared with anhydrous forsterite (Table 1). Both C_{ij} and Eulerian-angle parameters were varied in the fitting until a satisfactory and self-consistent fit was attained. For hy-Fo_{100}, the fitted orientations match the plate directions from X-ray diffraction within 0.1 (*hkl*) in the plane with higher anisotropy (010), and to within about 0.3 (*hkl*) for the plane with lowest anisotropy (100), shown in Figure 1a. In total, we measured six platelets of hy-Fo_{97}. The best self-consistency was

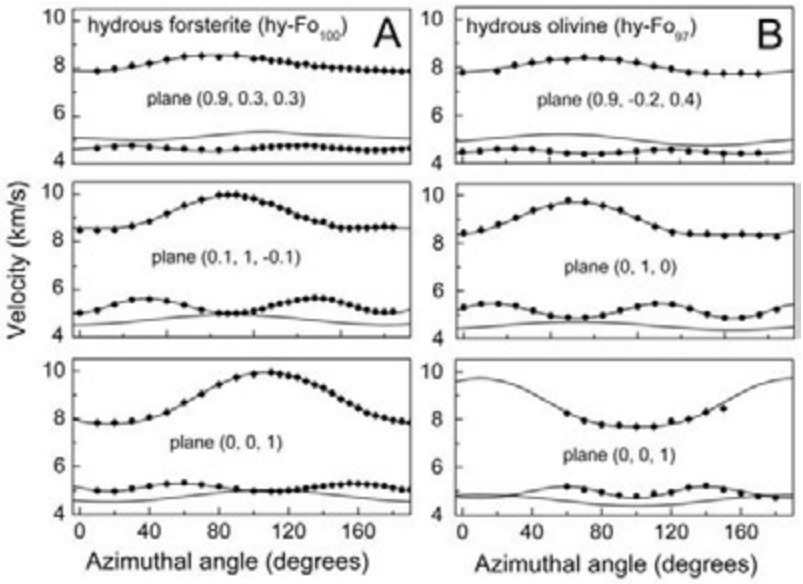

Figure 1. Measured acoustic velocities (filled symbols) as a function of azimuthal angle in three different plates for each composition, (a) hy-Fo_{100} and (b) hy-Fo_{97}. Fitted solutions to the Christoffel equations [*Every*, 1980] are shown by solid lines.

obtained using the *b*-plate, *c*-plate, and a random plate of fitted orientation (−0.9, −0.2, 0.4), shown in Figure 1b.

[10] The elastic constants of hy-Fo_{100} and hy-Fo_{97} are presented in Table 1, along with data for anhydrous forsterite [*Suzuki et al.*, 1983] and San Carlos olivine [*Webb*, 1989] for comparison. Aggregate bulk and shear moduli were calculated from the fitted elastic constants using the Voigt-Reuss-Hill average. Referring to Table 1, the addition of 10 mol% iron to pure-Mg forsterite reduces elastic constants with C_{ij} ($i = j$) by about 1–5%, whereas all

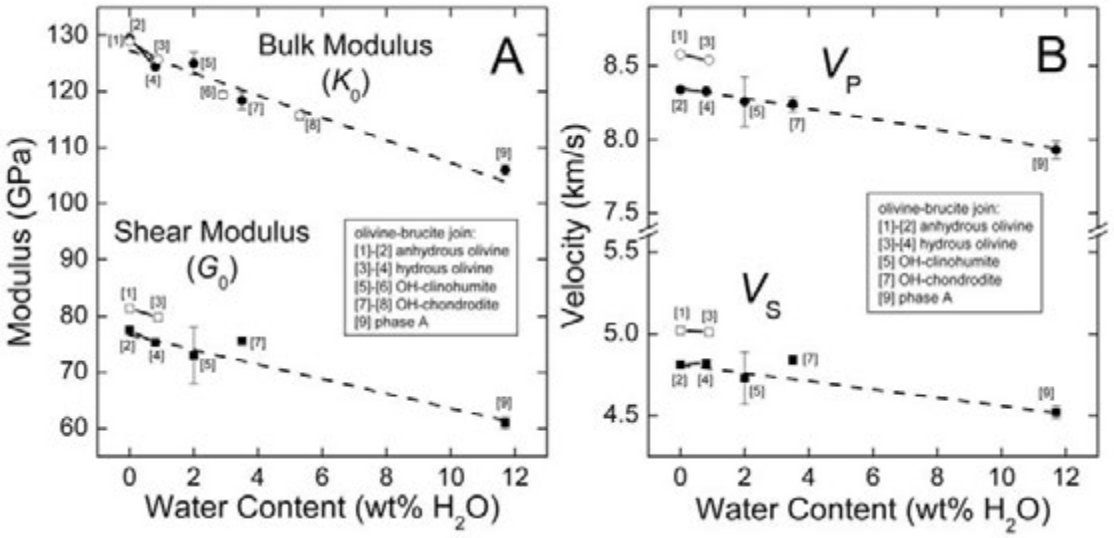

Figure 2. (a) Plot of bulk (K_0) and shear (G_0) moduli of minerals along the olivine-brucite join. (b) Plot of compressional (Vp) and shear (Vs) velocities of minerals along the olivine-brucite join. [1] anhydrous Fo_{100}, *Suzuki et al.* [1983]; [2] San Carlos olivine, *Webb* [1989]; [3] hy-Fo_{100}, this study; [4] hy-Fo_{97}, this study; [5] OH-clinohumite, $Mg_{8.2}Fe_{0.6}Si_4O_{16}(F_{0.29}OH_{0.71})_2$, *Fritzel and Bass* [1997]; [6] OH-clinohumite, $Mg_9Si_4O_{16}(OH)_2$, *Ross and Crichton* [2001]; [7] OH-chondrodite, $Mg_{4.7}Fe_{0.3}Si_2O_8(F_{0.31}OH_{0.67})_2$, *Sinogeikin and Bass* [1999]; [8] OH-chondrodite, $Mg_5Si_2O_8(OH)_2$, *Ross and Crichton* [2001]; [9] Phase A, $Mg_{6.85}Fe_{0.14}Si_2O_8(OH)_6$, *Sanchez-Valle et al.* [2006]. Fitted trends (dashed lines) are given in the text. Solid lines connect the two available data for olivine phases, provided in Table 1. Filled symbols are used for Fe-bearing compositions and open symbols are used for Mg-end member compositions.

Table 2. Anisotropy of Single-Crystal Olivine With Varying Iron and Water Content

	Forsterite[a]	San Carlos Olivine[b]	Hy-Fo_{100} This study	Hy-Fo_{97} This study
		P-Wave Anisotropy		
Vp[100][c]	10.09	9.78	9.96	9.73
Vp[010]	7.88	7.65	7.84	7.70
Vp[001]	8.55	8.35	8.59	8.37
%Anisotropy[d]	25.1(±0.4)	24.8(±0.3)	24.1(±0.4)	23.6(±0.8)
		S-Wave Anisotropy		
Vs // *a*-axis				
Polarized [010]	5.01	4.83	4.97	4.70
Polarized [001]	5.02	4.79	5.02	4.85
% anisotropy[d]	0.2(±0.3)	0.8(±0.3)	0.9(±0.5)	3.2(±1.2)
Vs // *b*-axis				
Polarized [100]	5.01	4.83	4.97	4.70
Polarized [001]	4.56	4.35	4.56	4.37
% anisotropy[d]	9.4(±0.3)	10.3(±0.4)	8.8(±0.7)	7.2(±1.5)
Vs // *c*-axis				
Polarized [100]	5.02	4.79	5.02	4.85
Polarized [010]	4.56	4.35	4.56	4.37
% anisotropy[d]	9.6(±0.4)	9.6(±0.5)	9.7(±0.5)	10.4(±1.3)
		LPO Analysis		
A-type fabric[e]				
V_{SH}	5.02	4.79	5.02	4.85
V_{SV}	5.01	4.83	4.97	4.70
V_{SH}/V_{SV}	1.002	0.992	1.009	1.032
B-type fabric[e]				
V_{SH}	5.02	4.79	5.02	4.85
V_{SV}	4.56	4.35	4.56	4.37
V_{SH}/V_{SV}	1.101	1.100	1.101	1.109
C-type fabric[e]				
V_{SH}	4.56	4.35	4.56	4.37
V_{SV}	5.02	4.79	5.02	4.85
V_{SH}/V_{SV}	0.908	0.909	0.908	0.901
E-type fabric[e]				
V_{SH}	5.01	4.83	4.97	4.70
V_{SV}	5.02	4.79	5.02	4.85
V_{SH}/V_{SV}	0.998	1.008	0.991	0.969

[a] *Suzuki et al.* [1983].
[b] *Webb* [1989].
[c] Uncertainties in velocities are 0.01–0.02 km/s, propagated from uncertainties in C_{ij}.
[d] Anisotropy (%) is calculated as [(Vmax − Vmin)/Vmean] × 100.
[e] Assumes horizontal flow, S-wave propagating in the shear plane, parallel to shear direction, with V_{SH} polarized in the shear plane, and V_{SV} polarized perpendicular to the shear plane. The crystal orientation for each fabric type is idealized using observed lattice preferred orientation (LPO) fabric types given by *Jung et al.* [2006].

off-diagonal terms of the tensor C_{ij} ($i \neq j$) increase by about 2–8%. The addition of 0.89 wt% H_2O to forsterite in our hy-Fo_{100} samples shows a reduction of all C_{ij} by 0.6–4.0%. For hy-Fo_{100}, we obtain K_{S0} = 125.7(±0.2) GPa and G_0 = 79.8(±0.1) GPa, which are about 2.5% and 2.0% lower than anhydrous forsterite, respectively.

[11] Comparing the C_{ij} of hy-Fo_{97} with anhydrous Fo_{100} to ascertain the net effect of iron and hydration shows that there is a large reduction in most C_{ij} by 4–12%, except for C_{13} and C_{23}, which are unchanged within error. For hy-Fo_{97}, we obtain K_{S0} = 124.4(±0.4) GPa and G_0 = 75.3(±0.3) GPa, which are 3.5% and 7.5% lower than anhydrous forsterite. The overriding trend is that addition of iron to forsterite has minimal or slightly positive effect on K_{S0}, but strongly reduces G_0, whereas the addition of water reduces both. Compared with pure-forsterite, addition of ~10 mol% Fe in San Carlos olivine reduces Vp and Vs by 2.8% and 4.2% respectively (Table 1). The hy-Fo_{97} velocities (with only 3 mol% Fe) are 2.9% and 4.0% lower than anhydrous forsterite, suggesting that hydrous Fo_{90} olivine, closer to mantle composition, would exhibit even further reduced velocities.

[12] The effects of water on elastic moduli and acoustic velocities of olivine are plotted in Figure 2, along with other minerals of the olivine-brucite join, $n[Mg_2SiO_4] \cdot Mg(OH)_2$, where n = 2 for chondrodite, n = 4 for clinohumite, and $Mg(OH)_2$ is the mineral brucite. In Figure 2, pure-Mg compositions are plotted with open symbols, and filled symbols are used for Fe-bearing compositions. Because the effects of iron on bulk moduli are small, we fitted a linear variation of bulk modulus with water content using all the data, shown by the dashed line in Figure 2a:

$$K_0(\text{GPa}) = 127.3(\pm 0.8) - 2.0(\pm 0.2) C_{H2O} \quad (2)$$

where C_{H2O} is the water content in weight percent. Because iron has a large influence on shear moduli, we fitted a linear variation of shear modulus with water content separately for Fe-bearing phases along the olivine-brucite join yielding,

$$G_0(\text{GPa}) = 76.6(\pm 0.6) - 1.3(\pm 0.1) C_{H2O}. \quad (3)$$

In Figure 2b, we show linear trends for the compressional and shear wave velocities for iron-bearing phases along the olivine-brucite join, resulting in:

$$\mathrm{Vp(km/s)} = 8.35(\pm 0.01) - 0.035(\pm 0.002) C_{\mathrm{H2O}} \quad (4)$$

$$\mathrm{Vs(km/s)} = 4.81(\pm 0.02) - 0.025(\pm 0.003) C_{\mathrm{H2O}}. \quad (5)$$

4. Anisotropy

[13] Seismic-wave anisotropy is one of the most robust geophysical observations used to infer flow geometry in the mantle. If orthorhombic olivine crystals align in lattice preferred orientation (LPO) under a given flow field, several types of anisotropy can occur. Although LPO studies have not been carried out at conditions relevant to the deep upper mantle with such high water contents, here we analyze the current results for various known types of LPO. In a horizontal flow field, P-waves travelling vertically through the field will exhibit slower velocities than P-waves propagating parallel to flow, called P*n*-type anisotropy, if the fast Vp[100] axis of olivine is preferentially aligned parallel to the flow, as in A-type LPO [e.g., *Jung et al.*, 2006]. The effects of iron and hydration on Vp in various crystallographic directions of olivine are listed in Table 2. Hydration of forsterite slightly reduces the maximum P-wave anisotropy, expressed as [(Vmax − Vmin)/Vmean] × 100, from 25.1 (±0.4)% to 24.1(±0.1)%. The hy-Fo_{97} sample shows further reduced P-wave anisotropy of 23.6(±0.4)%.

[14] In order to analyze the effects of hydration on shear-wave splitting anisotropy, we consider the idealized case of a single crystal aligned in a horizontal flow field with S-waves propagating in the plane of shear and polarized either in the shear plane (V_{SH}) or perpendicular to the shear plane (V_{SV}). In Table 2, Vs is given for each of the two possible pure-mode polarization directions for a given propagation direction parallel (//) to the *a*-axis, *b*-axis, and *c*-axes of olivine. The S-wave splitting anisotropy for anhydrous forsterite and San Carlos olivine with Vs // *b*- and *c*-axes is ∼10%, whereas S-waves propagating along the *a*-axis of olivine show little or no shear-wave splitting anisotropy, which is why this direction is chosen as the axis of symmetry in hexagonal transverse isotropy. Compared with anhydrous forsterite, the results for hy-Fo_{100} show hydration increases the S-wave splitting anisotropy from about 0.2% to 0.9% in the *a*-axis direction, but reduces S-wave splitting from about 9.4% to 8.8% for S-waves propagating in the *b*-axis direction, although we note that these differences are not drastic considering experimental uncertainty. The hy-Fo_{100} exhibits similar S-wave splitting anisotropy in the *c*-axis direction as anhydrous forsterite.

[15] In addition to type-A fabric associated with low-water conditions, *Jung et al.* [2006] described three newly observed fabric types; type-B associated with high-stress and/or moderate to high water contents, type-C associated with low-stress and water-rich conditions, and type-E associated with low-stress and moderate water contents. In Table 2, V_{SH} and V_{SV} are given for an idealized single-crystal oriented according to each of the observed fabric types reported by *Jung et al.* [2006]. Under horizontal shear (used to reference V_{SH} and V_{SV}, above), the hy-Fo_{97} olivine shows about 3% increase in shear-wave splitting anisotropy in idealized LPO type-A and type-E compared with dry forsterite (i.e. V_{SH}/V_{SV} increases from about 1.00 to 1.03) because both type-A and type-E fabrics have [100] subparallel to the direction of shear. Type-A and type-E fabrics, however, are associated with low-to-moderate water contents (and/or low stress). Under more water-rich conditions, *Jung et al.* [2006] report type-B (high stress) and type-C (low stress) fabrics, both of which exhibit preferred *c*-axis alignment sub-parallel to the shear direction. In both cases (type-B and type-C) there is essentially no change in S-wave splitting anisotropy with hydration (Table 2) but because the *c*-axis is sub-parallel to flow, the P*n*-type anisotropy would instead show fast vertical propagating P-waves compared with the direction of shear. In the case that type-A fabric persisted under hydrous conditions, P*n*-type anisotropy would still display fast P-waves in the direction of shear, but S-wave splitting anisotropy would be greater than under anhydrous conditions. Future studies of LPO at deeper mantle pressures and under more hydrous conditions are needed to determine what type of LPO might be relevant near the transition zone. In addition, pressure and temperature derivatives of the elastic moduli of hydrous olivine are needed in order to provide a more robust prediction of possible seismological signatures of hydration in the deep upper mantle.

[16] **Acknowledgments.** This research was supported by the NSF (EAR-0748707 to S. D. Jacobsen and EAR-0738510 to T. S. Duffy), the Carnegie/DOE Alliance Center (CDAC), the Alexander von Humboldt Foundation, and the Bayerishes Geoinstitut Visitors Program.

References

Bell, D. R., G. R. Rossman, J. Maldener, D. Endisch, and F. Rauch (2003), Hydroxide in olivine: A quantitative determination of the absolute amount and calibration of the IR spectrum, *J. Geophys. Res.*, *108*(B2), 2105, doi:10.1029/2001JB000679.

Every, A. G. (1980), General closed-form expressions for acoustic waves in elastically anisotropic solids, *Phys. Rev. B*, *22*, 1746–1760.

Fritzel, T. L. B., and J. D. Bass (1997), Sound velocities of clinohumite, and implications for water in Earth's upper mantle, *Geophys. Res. Lett.*, *24*, 1023–1026.

Hauri, E. H., G. A. Gaetani, and T. H. Green (2006), Partitioning of water during melting of the Earth's upper mantle at H_2O-undersaturated conditions, *Earth Planet. Sci. Lett.*, *248*, 715–734.

Hirth, G., and D. L. Kohlstedt (1996), Water in the oceanic upper mantle: Implications for rheology, melt extraction and the evolution of the lithosphere, *Earth Planet. Sci. Lett.*, *144*, 93–108.

Jacobsen, S. D. (2006), Effect of water on the equation of state of nominally anhydrous minerals, *Rev. Mineral. Geochem.*, *62*, 321–342.

Jacobsen, S. D., and J. R. Smyth (2006), Effect of water on the sound velocities of ringwoodite in the transition zone, in *Earth's Deep Water Cycle*, *Geophys. Monogr. Ser.*, vol. 168, edited by S. D. Jacobsen and S. van der Lee, pp. 131–145, AGU, Washington, D. C.

Jung, H., I. Katayama, Z. Jiang, T. Hiraga, and S. Karato (2006), Effect of water and stress on the lattice-preferred orientation of olivine, *Tectonophysics*, *421*, 1–22.

Karato, S. (1993), Importance of anelasticity in the interpretation of seismic tomography, *Geophys. Res. Lett.*, *20*, 1623–1626.

Karato, S., and H. Jung (1998), Water, partial melting and the origin of the seismic low velocity and high attenuation zone in the upper mantle, *Earth Planet. Sci. Lett.*, *157*, 193–207.

Lemaire, C., S. C. Kohn, and R. A. Brooker (2004), The effect of silica activity on the incorporation mechanisms of water in synthetic forsterite: A polarized infrared spectroscopic study, *Contrib. Mineral. Petrol.*, *147*, 48–57.

Litasov, K. D., E. Ohtani, H. Kagi, S. D. Jacobsen, and S. Ghosh (2007), Temperature dependence and mechanism of hydrogen incorporation in olivine at 12.5–14.0 GPa, *Geophys. Res. Lett.*, *34*, L16314, doi:10.1029/2007GL030737.

Mao, Z., S. D. Jacobsen, F. Jiang, J. R. Smyth, C. M. Holl, D. J. Frost, and T. S. Duffy (2008), Single-crystal elasticity of wadsleyites, β-Mg_2SiO_4, containing 0.37–1.66 wt.% H_2O, *Earth Planet. Sci. Lett.*, *268*, 540–549.

Mei, S., and D. L. Kohlstedt (2000), Influence of water on plastic deformation of olivine aggregates, *J. Geophys. Res.*, *105*, 21,457–21,469.

Mosenfelder, J. L., N. I. Deligne, P. D. Asimow, and G. R. Rossman (2006a), Hydrogen incorporation in olivine from 2–12 GPa, *Am. Mineral.*, *91*, 285–294.

Mosenfelder, J. L., T. G. Sharp, P. D. Asimow, and G. R. Rossman (2006b), Hydrogen incorporation in natural mantle olivines, in *Earth's Deep Water Cycle*, *Geophys. Monogr. Ser.*, vol. 168, edited by S. D. Jacobsen and S. van der Lee, pp. 45–56, AGU, Washington, D. C.

Ross, N. L., and W. A. Crichton (2001), Compression of synthetic hydroxylclinohumite [$Mg_9Si_4O_{16}(OH)_2$)] and hydroxylchondrodite [$Mg_5Si_2O_8(OH)_2$], *Am. Mineral.*, *86*, 990–996.

Sanchez-Valle, C., S. V. Sinogeikin, J. R. Smyth, and J. D. Bass (2006), Single-crystal elastic properties of dense hydrous magnesium silicate phase A, *Am. Mineral.*, *91*, 961–964.

Simpson, F., and A. Tommasi (2005), Hydrogen diffusivity and electrical anisotropy of a peridotite mantle, *Geophys. J. Int.*, *160*, 1092–1102.

Sinogeikin, S. V., and J. D. Bass (1999), Single-crystal elastic properties of chondrodite: Implications for water in the upper mantle, *Phys. Chem. Minerals*, *26*, 297–303.

Sinogeikin, S. V., T. Katsura, and J. D. Bass (1998), Sound velocities and elastic properties of Fe-bearing wadsleyite and ringwoodite, *J. Geophys. Res.*, *103*, 20,819–20,825.

Smyth, J. R., D. J. Frost, F. Nestola, C. M. Holl, and G. Bromiley (2006), Olivine hydration in the deep upper mantle: Effects of temperature and silica activity, *Geophys. Res. Lett.*, *33*, L15301, doi:10.1029/2006GL026194.

Suzuki, I., O. L. Anderson, and Y. Sumino (1983), Elastic properties of a single-crystal forsterite Mg_2SiO_4, up to 1,200 K, *Phys. Chem. Minerals*, *10*, 38–46.

Wang, J., S. V. Sinogeikin, T. Inoue, and J. D. Bass (2006), Elastic properties of hydrous ringwoodite at high-pressure conditions, *Geophys. Res. Lett.*, *33*, L14308, doi:10.1029/2006GL026441.

Webb, S. L. (1989), The elasticity of the upper mantle orthosilicates olivine and garnet to 3 GPa, *Phys. Chem. Minerals*, *16*, 684–692.

Zhao, Y.-H., S. B. Ginsberg, and D. L. Kohlstedt (2004), Solubility of hydrogen in olivine: Dependence on temperature and iron content, *Contrib. Mineral. Petrol.*, *147*, 155–161.

T. S. Duffy, F. Jiang, and Z. Mao, Department of Geosciences, Princeton University, Princeton, NJ 08544, USA.

D. J. Frost, Bayerisches Geoinstitut, University of Bayreuth, D-95440 Bayreuth, Germany.

C. M. Holl and S. D. Jacobsen, Department of Earth and Planetary Sciences, Northwestern University, Evanston, IL 60208, USA. (steven@earth.northwestern.edu)

J. R. Smyth, Department of Geological Sciences, University of Colorado, Boulder, CO 80309, USA.